Marine Pollution Bulletin 225 (2026) 119293

Contents lists available at ScienceDirect

Marine Pollution Bulletin

journal homepage: www.elsevier.com/locate/marpolbul

Multi-omics reveal the prevalence of Thaumarchaeota and their biogeochemical roles in coastal low oxygen zones

Yu Han [a], Airui Wang [a], Zhijie Zhang [a], Le Liu [a], Quanrui Chen [b], Wei Fan [c], Ehui Tan [a,*], Kai Tang [b,*]

[a] School of Marine Sciences, State Key Laboratory of Marine Resource Utilization in South China Sea, Hainan University, Haikou, Hainan, China
[b] State Key Laboratory of Marine Environmental Science, Xiamen University, Xiamen, China
[c] Institute of Ocean Engineering & Technology, Ocean College, Zhejiang University, Zhoushan, China

ARTICLE INFO

Keywords:
East China Sea
Deoxygenation
Metagenomic
Metaproteomic
Thaumarchaeota

ABSTRACT

The intensification of coastal hypoxia under anthropogenic eutrophication and climate change necessitates understanding microbial adaptive mechanisms. However, the composition of microbial communities and their biogeochemical roles in response to oxygen gradients remain poorly understood. Here, we employed integrated multi-omics approaches to analyze microbial communities and their biogeochemical functions across oxic to low oxygen gradients off the Yangtze River Estuary in East China Sea. Results revealed that surface oxic waters hosted phytoplankton (*Synechococcus*) and opportunistic bacteria (Flavobacteriia, Pelagibacterales), while bottom layers enriched chemolithoautotrophs (Thaumarchaeota, Nitrospina) and facultative anaerobes (Planctomycetes, Marine Group II), with sediment resuspension further amplified particle-attached taxa. Meanwhile, a remarkable shift in microbial nitrogen metabolism was observed between oxic and low oxygen waters, with dissolved nitrogen assimilation dominated in oxic waters. Despite genomic potential for complete nitrogen reduction in low oxygen waters, our metaproteomics revealed only a significant expression of nitrate reductases. This decoupling between genomic potential and proteomic expression implies that ambient oxygen levels remain above thresholds for full pathway activation, showcasing microbial metabolic plasticity. Both metagenomic and metaproteomic have confirmed that Thaumarchaeota, particularly the genus *Nitrosopumilus*, emerged as keystone taxa, contributing to nitrification and dark carbon fixation, thereby coupling nitrogen-carbon biogeochemical cycling in coastal hypoxic zones. These findings highlight redox-driven microbial niche differentiation and metabolic adaptation, providing predictive insights into biogeochemical feedbacks under expanding coastal deoxygenation.

1. Introduction

Dissolved oxygen (DO) is a critical environmental factor in marine ecosystems, with its spatial heterogeneity and vertical stratification fundamentally establishing the biogeochemical zonation of redox boundaries (Wang et al., 2024). DO controls the predominance of aerobic versus anaerobic metabolic pathways, thereby structuring microbial community assemblages and modulating energy transfer efficiency across trophic levels (Song et al., 2019). Under the pressures of climate warming and anthropogenic eutrophication, the global expansion of coastal hypoxic zones (DO <2 mg/L) and oceanic oxygen minimum zones has been documented with increasing concern (Breitburg et al., 2018; Oschlies, 2021). The ocean deoxygenation imposes physiological constraints on aerobic biota through habitat compression, leading to systematic biodiversity erosion and functional homogenization (Rose et al., 2024), destabilizing energy flux patterns and nutrient cycling regimes (Long et al., 2021). Such alterations progressively impair ecosystem services, ultimately threatening the resilience and long-term sustainability of marine ecosystems.

Microorganisms act as fundamental biogeochemical engineers in marine systems (Sun, 2024). They orchestrate elemental biogeochemical cycles and maintain ecosystem homeostasis through coupled metabolic networks, while also regulating global climate via production/consumption of greenhouse gases (He et al., 2023). The expansion of oxygen-depleted zones creates oxic-anoxic gradient along the water column, triggering profound restructuring of microbial communities

* Corresponding authors.
E-mail addresses: ehuitan@hainanu.edu.cn (E. Tan), tangkai@xmu.edu.cn (K. Tang).

https://doi.org/10.1016/j.marpolbul.2026.119293
Received 13 August 2025; Received in revised form 12 January 2026; Accepted 13 January 2026
0025-326X/© 2026 Elsevier Ltd. All rights are reserved, including those for text and data mining, AI training, and similar technologies.

(Lin et al., 2025), which in turn alters the mediated carbon and nitrogen cycling processes, resulting in a series of environmental and climatic feedbacks (Sveen et al., 2024). Typically, photoautotrophic phytoplankton dominate the oxygenated surface layer and participate in carbon dioxide fixation (Avrahami et al., 2025). As depth increases and DO declines, chemolithoautotrophs and facultative anaerobes become the dominant functional groups (Han et al., 2022). This transition is primarily reflected in the nitrogen cycle pathways, shifting from assimilation-dominated to nitrate reduction processes, synchronously driving nitrogen transformation and dark carbon fixation, thereby coupling carbon and nitrogen cycles (Tang et al., 2025). Meanwhile, heterotrophic microorganisms are widely distributed throughout the water column, participating in the mineralization of organic matter and providing inorganic nutrients to other microbes (Chen et al., 2025). This metabolic adaptation not only optimizes energy acquisition strategies for microorganisms in low-oxygen environments, but also regulates greenhouse gas fluxes and organic carbon export, forming critical biogeochemical feedbacks that ultimately influence the global climate system (Sveen et al., 2024). Deciphering microbial adaptation mechanisms under oxygen stress has emerged as a hotspot in marine microbiology, with implications for predicting biogeochemical feedbacks under expanding marine deoxygenation.

Among these microbes, the Thaumarchaeota phylum, comprising all currently described ammonia-oxidizing archaea (Offre et al., 2013), constitutes a pivotal microbial group, accounting for 20–50% of pelagic archaeal populations across all oceanic provinces (Qin et al., 2020; Stahl and De La Torre, 2012). Among the primary ecotypes of Thaumarchaeota, the genera *Nitrosopumilus* is the only broadly adaptable lineage capable of thriving in diverse habitats, including freshwater, estuarine environments, hypoxic zones and from surface to abyssal waters (Liu et al., 2023; Zhang et al., 2024a), demonstrating varied adaptive strategies across environmental gradients (Qin et al., 2020). Particularly in nutrient-rich estuarine ecosystems, *Nitrosopumilus* functions as a chemolithoautotrophic opportunist, effectively occupying a distinct ecological niche. Estuarine ecosystems typically receive substantial terrestrial nutrient inputs and experience intense sediment resuspension, creating favorable conditions for the proliferation of photoautotrophs and heterotrophic bacteria, which compete for inorganic nitrogen and organic matter, respectively (Han et al., 2022). Facing such a complex and competitive environment, *Nitrosopumilus* possesses unique adaptive strategies, including high affinity for ammonium (Straka et al., 2019), broad salinity tolerance (Qin et al., 2017), and the expression of ammonium transporters and nitrite reductase to facilitate nitrogen acquisition (Reyes et al., 2020). Additionally, the 3-hydroxypropionate/4-hydroxybutyrate cycle for chemolithoautotrophic carbon fixation, synergistic interactions with heterotrophic bacteria (which decompose organic nitrogen to release ammonium as a substrate for *Nitrosopumilus*), and enhanced antioxidant capacity (Han et al., 2022) collectively support their survival and prevalence. Due to substrate competition and light inhibition (Wan et al., 2021), the ecological niches of Thaumarchaeota and photoautotrophs are often vertically separated, as light intensity decreases and photoautotrophic activity declines, Thaumarchaeota gradually play the critical ecological roles in nitrogen biogeochemical cycle and chemolithoautotrophic carbon fixation (Qin et al., 2020). As keystone nitrifiers, Thaumarchaeota govern nitrogen speciation particularly in oligotrophic gyres (Semedo et al., 2021). In addition, their chemolithoautotrophic metabolism establishes them as major contributors to dark carbon fixation (Martens-Habbena and Qin, 2022). Furthermore, they are largely involved in the production and consumption of nitrous oxide and methane (Wan et al., 2023), biologically linking the microbial-scale processes with planetary-scale climate dynamics.

Although an increasing number of studies are investigating microbial community composition and their biogeochemical functions in response to deoxygenation across various spatial and temporal scales (Lin et al., 2025; Sun, 2024). However, the adaptive mechanisms of specific microbial taxa (such as Thaumarchaeota) to marine oxygen fluctuations, particularly the transition from oxic to anoxic, and their associated biogeochemical roles remain poorly understood. Driven by anthropogenic eutrophication and climate warming, the Yangtze River Estuary and adjacent East China Sea have been experiencing seasonal hypoxia from May to November annually, with peak intensity in August when average dissolved oxygen in the core zone can decrease to as low as 1.5 mg/L (Sheng et al., 2024; Zhang et al., 2023). By applying an integrated multi-omics approach (16S rRNA gene sequencing, metagenomics, and metaproteomics), we conduct comparative analyses of microbial community structures and functional gene expression across oxic-low oxygen gradients in East China Sea to (1) elucidate the dynamic shifts in microbial taxonomic diversity along oxygen gradients and (2) reveal the metabolic responses and adaptation mechanisms of key microbial groups, particularly Thaumarchaeota, under deoxygenation stress.

2. Experimental procedures

2.1. Sample collection and preservation

The sampling cruise was conducted on July 25–26, 2020 in the seasonal hypoxic zone off the Yangtze River Estuary (Fig. 1). Seawater samples were collected for nutrient and microbial analysis at site C1 (30.12°N, 122.74°E) by using 10 L Niskin bottles attached to a conductivity-temperature-depth (CTD) rosette sampler. To measure nitrate (NO_3^--N), nitrite (NO_2^--N), ammonium (NH_4^+-N), dissolved inorganic phosphorus (DIP), and dissolved silicon (DSi), water samples were collected via 0.45 μm membrane at five layers, with depths of 0.5 m (C1T), 5 m (C1S), 15 m (C1M), 40 m (C1L) and 50 m (C1B). Based on the dissolved oxygen (DO) profile measured in the field, nearly 100 L of seawater was collected at both surface (5 m, aerobic, C1S) and bottom (50 m, low oxygen, C1B) layers for prokaryotes (<3 μm; (Teeling et al., 2012)) analysis. Briefly, seawater was successively passed through a 20 μm screen and a 3 μm polycarbonate filter membrane (142 mm, Merck, Germany), then ~10 L of filtrate was further filtered via a 0.22 μm polycarbonate filter membrane (47 mm, Merck, Germany) for high-throughput 16S rRNA gene sequencing and metagenomics analysis (Genomics BioTech). For metaproteomic analysis, the other 90 L of filtrate was filtered using Sterivex-GV pressure filter protein tubule (0.22 μm, Merck, Germany) and then 1.8 mL of lysis buffer (0.75 mol L^{-1} sucrose, 40 mmol L^{-1} EDTA, 50 mmol L^{-1} Tris, pH = 8.3) was added to protein tubules (Hawley et al., 2013). Additionally, the filtrate filtered through a 20 μm screen was collected and stored with 1% glutaraldehyde at −80 °C for the determination of the total abundance of prokaryotes.

2.2. Chemical measurements

Seawater temperature, salinity, DO, chlorophyll *a* (Chl a) and turbidity were measured in situ by using the corresponding probe carried by CTD, and DO concentrations were corrected by the Winkler method-derived measurements. The concentrations of NO_3^--N, NO_2^--N, NH_4^+-N, DIP and DSi were determined by the AA3 continuous flow analyzer (Dai et al., 2008).

2.3. Prokaryotic abundance measurements

The abundance of prokaryotes, mainly including archaea and bacteria was detected by using Flow CytoMetry (Jiao et al., 2002). The data were analyzed by FCS Express software, and samples were distinguished according to cell size, granularity, chlorophyll *a*nd other parameters. The distribution area of the scatter plot of the instrument was manually delineated. The cell number of the circle plot was automatically counted by the software, and the cell abundance of the sample was calculated as follows,

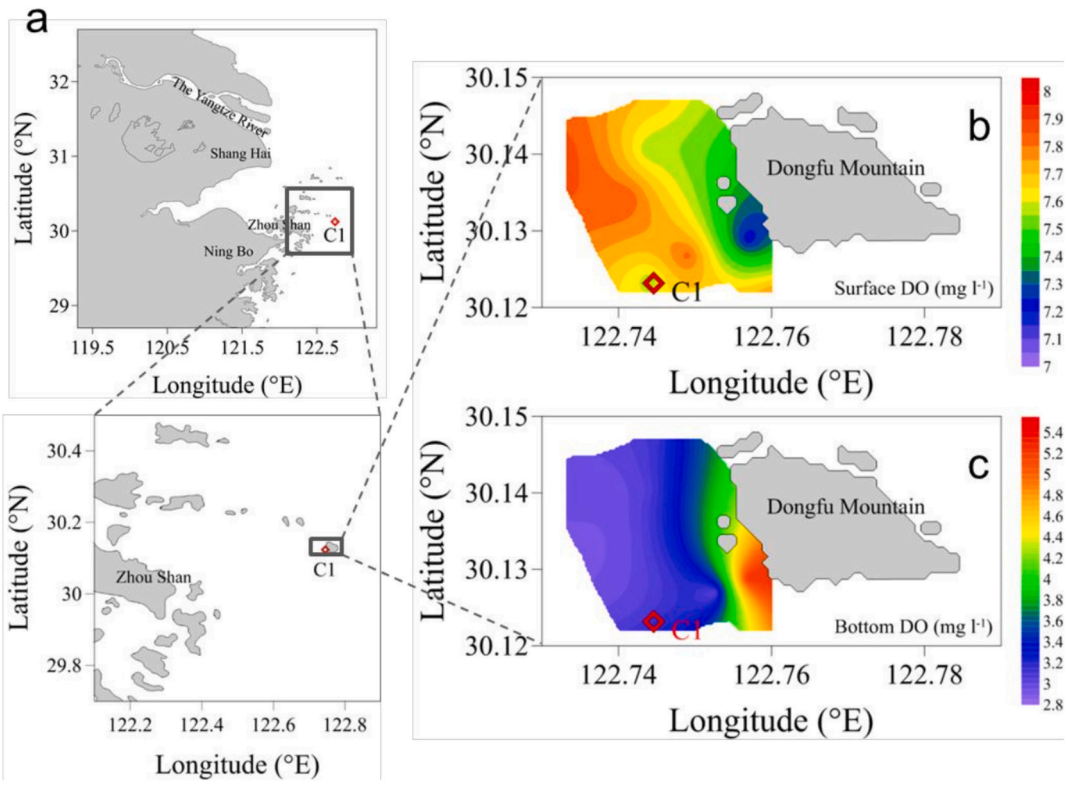


Fig. 1. The sampling site in (a) hypoxic zone, East China Sea, with dissolved oxygen in surface and bottom water showing in (b) and (c), respectively.

$$C = \frac{3600 \times N \times Vol_{total}}{V \times T \times Vol_{sample}} \quad (1)$$

where C is the cell abundance of prokaryotes (cells mL^{-1}); N is the number of cells detected by the instrument; V and T are injection flow rate (mL h^{-1}) and flow analysis time (s), respectively. Vol_{sample} stands for sample volume (mL); Vol_{total} is the total volume (mL) of the test sample.

2.4. Sequencing of high-throughput 16S rRNA genes and data processing

For the relative quantification, microbial community genomic DNA was extracted using the soil genomic DNA extraction Kit (DNeasy PowerSoil Kit, MoBio, USA). PCR amplification of the V4 variable region of the 16S rRNA genes in archaea and bacteria was performed using modified 515F mod (5'-GTGYCAGCMGCCGCGGTAA-3′) and 806R mod (5'-GGACTACNVGGGTWTCTAAT-3′) primers (Walters et al., 2016). The PCR products were then recovered with 2% agarose Gel and purified by AxyPrep DNA Gel Extraction Kit (Axygen Biosciences, Union City, CA, USA). After agarose gel electrophoresis, the product was quantified with Quantus™ Fluorometer (Promega, USA), and then quantified with the NEXTFLEX Rapid DNA-Seq Kit. Finally, it was sequenced by Illumina Miseq platform (Han et al., 2022). For the absolute quantification of 16S rRNA genes, 2–3 of spike-in sequences are inserted into the DNA sample pool with four different concentration gradients of 10^3, 10^4, 10^5, and 10^6 copy numbers for each sequence, and taken as an internal standard for absolute quantification and comparative analysis of samples (Jiang et al., 2019; Tkacz et al., 2018). The following amplification and sequence of 16S rRNA genes in archaea and bacteria were the same as aforementioned (Walters et al., 2016).

The original sequencing data were processed according to the description of Huang et al. (2015). Adaptor sequence and primer sequence were removed by TrimGalore and motherur, respectively. Double-ended reads were spliced and low-quality reads were discarded (< 200 bp, average quality score < 20, ambiguous base calls >0). The USEARCH (version 10) was used to cluster operational taxonomic units (OTUs), clustering sequences with similarity >97% into the same OTU classification unit (Huang et al., 2015). Species taxonomic annotation was performed by comparing the RDP v11.5 database with the command classify.seqs of Mothur v1.41.1 and by setting a confidence threshold of 80%. The absolute quantitative copy number of the prokaryotic OTUs was calculated from the standard curve established by the copy number of the OTU containing the spike-in sequence. The raw data were stored in the NCBI Sequence Read Archive (SRA) with entry numbers SRR11179217-SRR11179228.

2.5. Metagenomics analysis

Sample DNA was extracted from the QIAGEN Large-Construct Kit (QIAGEN, Germany), and then purified by the QIAGEN DNe purification kit (QIAGEN, Germany). After purification, the samples were tested for Qubit® 2.0 Fluorometer (Invitrogen, USA) concentration and 1.2% agar-gel electrophoresis (80 V constant pressure, 40 min) to confirm that the DNA master band was clear with no RNA contamination. Following DNA extraction from the metagenome, detection was performed via electrophoresis on a 1% agarose gel. The DNA was fragmented using a Covaris M220 focused-ultrasonicator (Covaris, USA) and PE libraries were constructed using the TruSeq™ DNA Sample Prep Kit. Subsequently, bridge PCR amplification of the DNA fragments was conducted using the cBot Truseq PE Cluster Kit v3-cBot-HS. Finally, sequencing was performed on the Illumina NovaSeq 6000 platform employing the Truseq SBS Kit (300 cycles).

Following quality assessment of the raw sequence data using FastQC v0.11.9 (Thrash et al., 2018), adapter sequences were removed and reads were quality-trimmed using Trimmomatic v0.38 (Bolger et al., 2014) to generate clean reads. Taxonomic classification of the metagenomic data was subsequently performed using Kraken2 v2.1.1 with the Genome Taxonomy Database (GTDB, vR202; https://gtdb.ecogenomic.org/) classification system. Sequence assembly was conducted using the MEGAHIT assembler (https://github.com/voutcn/megahit). Protein-coding genes were then predicted from the assembled contigs

using METAProdigal (http://prodigal.ornl.gov/). The predicted gene sequences were clustered using CD-HIT (http://www.bioinformatics.org/cd-hit/) to construct a non-redundant gene catalog, with the longest sequence within each cluster serving as the representative gene. Gene abundance was quantified using Salmon (https://github.com/COMBINE-lab/salmon). Finally, the gene catalog was functionally annotated via BLASTP alignment against multiple reference databases, including the Non-Redundant Protein (NRP) Database, the Kyoto Encyclopedia of Genes and Genomes (KEGG) database, the evolutionary genealogy of genes: Non-supervised Orthologous Groups (eggNOG) database, and the Carbohydrate-Active enZymes (CAZy) database. This process yielded functional annotations, taxonomic annotations, and Clusters of Orthologous Groups (COG) functional classifications for the predicted genes.

To conduct the metagenomic assembly genomics and BLAST, the raw sequencing data were similarly processed using FastQC and Trimmomatic for quality control, followed by taxonomic classification of the metagenomic data based on the k-mer-based Kraken2 reference genome database. The quality-filtered sequences were then assembled using MetaSPAdes v3.15.2 with a minimum contig length threshold of 200 bp. High-quality reads were mapped to the assembled genomic sequences using Bowtie2 v2.3.4.3, and genome binning was performed on the assembly results using MetaBAT v2.12.1. The reconstructed genomes were subsequently evaluated with CheckM v1.0.7, and taxonomic annotation of the gene clusters were performed using GTDB-Tk v1.5.0. For BLAST analysis, seven selected bins were subjected to open reading frame (ORF) prediction using MetaProdigal v2.6.3. The predicted protein-coding genes were functionally annotated with eggNOG-mapper v2.1.6. The ORFs were then aligned against the custom-built DNA-seq reference library derived from the study area, and the number of mapped reads was calculated for each alignment.

2.6. Metaproteomics analysis

The proteins were extracted and the purity was evaluated by applying sodium dodecyl sulfate polyacrylamide gel electrophoresis (SDS-PAGE) (Hawley et al., 2013). The concentration of protein was determined by using BCA kit. By adding trypsin to the proteins, and peptides were obtained via enzymolysis. The peptides were then isolated and detected using the QExactive™ Plus mass spectrometry system (Thermo Scientific, USA) equipped with an ultra-high performance liquid chromatography (EASY-nLC 1000, Thermo Scientific, USA).

The metaproteomic data were processed using MaxQuant v1.6.15.0 for database searching against the custom database constructed from metagenomic assemblies of the Yangtze River Estuary. This custom database was constructed using all metagenomic contigs and contains approximately 1,590,301 non-redundant protein sequences, broadly covering the domains of bacteria and archaea. The overall functional gene annotation rate is 89.6%, and the coverage of key functional genes (annotated by the KEGG database) is 71.9%. Common contaminant databases were also included to eliminate the impact of contaminant proteins in identification results. Quality control was performed at both peptide and protein levels based on the database search results. The identified proteins were functionally annotated by using Gene Ontology (GO), Protein domain, KEGG, and COG classifications (Schiebenhoefer et al., 2020). In addition, quantitative analysis of proteins was performed, including quantitative distribution and repeatability analysis. Protein abundance was determined based on unique peptides and represented by LFQ intensity values correcting from the original intensity value of the protein.

3. Results

3.1. Environmental characteristics

During the sampling period, the temperature along the water depth remained constantly at ~24 °C (Fig. 2a), while the salinity increased gradually from 22.4 in surface water to 32.9 in bottom water (Fig. 2b). This low-salinity surface waters indicate the influence of the Changjiang Diluted Water. The concentration of Chl a in the upper water was generally high with a maximum of 941 ng L^{-1} at 20–30 m, and then decreased with the increase of the water depth (Fig. 2c). Both the concentration and saturation of DO showed a continuous decreasing trend with the increase of water depth. The DO concentration in surface water was saturated and then decreased to as low as 3.2 mg/L in bottom water, representing a transition level from oxic to anoxic conditions (Fig. 2d and Table 1). The turbidity remained basically stable at a depth of 35 m or less, and then increased with the increase of the water depth (Fig. 2e and Table 1). Overall, the concentrations of NO_3^--N, NO_2^--N, NH_4^+-N, DIP and DSi exhibited consistent vertical distribution patterns (Table 1). Their concentrations progressively decreased with increasing depth, reaching the minimum at a water depth of ~15 m. Below this depth, all nutrient showed slight increases with further depth progression. Among the dissolved inorganic nitrogen species, NO_3^--N was the predominant form, with concentrations of 4.5–29.9 μmol L^{-1}. NH_4^+-N represented the secondary component, while NO_2^--N consistently displayed the lowest concentrations throughout the water column (Table 1). The total abundance of prokaryotes in the whole water column ranged from 3.2 to 4.6 × 10^6 cells mL^{-1}, with a slightly higher abundance in deep water (Table 1).

3.2. Microbial community composition

A total of 2487 ASVs belonging to 26 phyla and 115 families were identified by high-throughput 16S rRNA gene sequencing (Table S3). From the perspective of phylum classification, the dominant microbes in the study area included Proteobacteria, Thaumarchaeota, Euryarchaeota, Bacteroidetes, Cyanobacteria, Actinobacteria, Planctomycetes, Verrucomicrobia and Nitrospinae, accounting for 88.7% of the total microbial abundance regardless of the sampling depth (Fig. 3a). Based on the vertical distribution of microbial communities, the absolute abundance of dominant microbial groups exhibited distinct patterns between surface and bottom water (Fig. 3b). Thaumarchaeota and Proteobacteria presented remarkable increases in absolute abundance by a factor of 2.5 and 1.7 from the oxygenated surface layer (3.8 × 10^5 copies mL^{-1} and 6.3 × 10^5 copies mL^{-1}, respectively) to the oxygen-depleted bottom layer (9.5 × 10^5 copies mL^{-1} and 1.1 × 10^6 copies mL^{-1}; Fig. 3b). Conversely, Cyanobacteria and Bacteroidetes exhibited significant decreases from 8.5 × 10^4 copies mL^{-1} and 1.1 × 10^5 copies mL^{-1} in the surface oxic waters to 8.2 × 10^3 copies mL^{-1} and 8.8 × 10^4 copies mL^{-1} in the low oxygen bottom layer, corresponding to reductions of approximately 90.4% and 16.9%, respectively (Fig. 3b). Furthermore, nitrite-oxidizing bacteria, including Nitrospina, Nitrobacter, and Nitrospira, consistently showed increased abundance in the bottom waters (Fig. 3b).

At the family level, the dominant microbial groups were Nitrosopumilaceae, GpIIa (*Synechococcus* and *Prochlorococcus*), Pelagibacteraceae, Rhodobacteraceae, Pseudoalteromonadaceae, Alteromonadaceae, Rhodospirillaceae, Flavobacteriaceae, Cryomorphaceae, and Nitrospinaceae, together contributing 56.0% and 61.2% of the total microbial abundance in surface and bottom water, respectively (Fig. 3e). In terms of vertical structure, with the increase of water depth, the abundance of Nitrosopumilaceae in the bottom deoxygenated water increased by 2.5-fold (from 3.8 × 10^5 to 9.5 × 10^5 copies mL^{-1}, Fig. 3f), while the photoautotrophic GpIIa family decreased by 90.5% (from 8.5 × 10^4 to 8.2 × 10^3 copies mL^{-1}, Fig. 3f). The abundance of Flavobacteriaceae and Cryomorphaceae in Bacteroidetes decreased by 9.2% and 67.2% in bottom water (Fig. 3f), respectively. For the Proteobacteria, the abundance of Rhodobacteraceae and Rhodospirillaceae showed a decrease pattern from surface to bottom water (Fig. 3f), while the abundance of Pseudoalteromonadaceae and Alteromonadaceae increased by 5 and 3 orders of magnitude, respectively

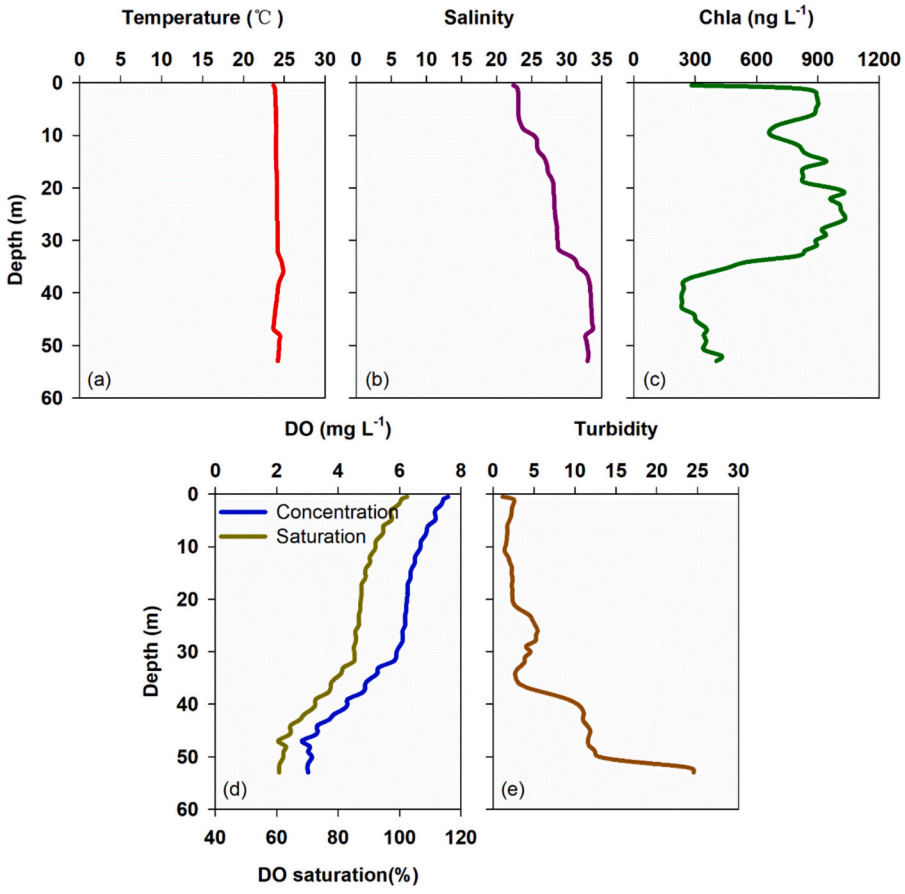


Fig. 2. The vertical distribution of temperature, salinity, chlorophyll a, dissolved oxygen, and turbidity at site C1 in deoxygenated area of East China Sea.

Table 1
The concentrations of dissolved and nutrients in different water depth at the deoxygenated sites (C1) in the East China Sea.
Abbreviations: DO, Dissolved oxygen; DIN: Dissolved inorganic nitrogen; DIP: Dissolved inorganic phosphate; DSi: Dissolved silicate; TPA: Total prokaryotic abundance.

Factors	C1T	C1S	C1M	C1L	C1B
Depth (m)	0.5	5	15	40	50
DO (mg/L)	7.6	7.2	6.4	4.3	3.2
DO (%)	102.5	97.3	88.8	72.6	62.2
NO_3^--N (μmol L^{-1})	29.9	15.9	6.2	4.5	5.8
NO_2^--N (μmol L^{-1})	0.7	0.5	0.2	0. 5	0.6
NH_4^+-N (μmol L^{-1})	2.6	1.9	0.02	2.2	2.5
DIN (μmol L^{-1})	33.2	18.3	6.42	7.2	8.9
DIP (μmol L^{-1})	0.7	0.4	0.2	0.4	0.3
DSi (μmol L^{-1})	35.6	22.6	9.9	9.6	10.4
TPA (10^6 cells mL^{-1})	–	3.2 ± 0.1	4.5 ± 0.6	–	4.6 ± 0.2

Note that "-" represent not applicable.

(Fig. 3f). In addition, the abundance of Nitrospinaceae and Planctomycetes also increased in bottom hypoxic water (Fig. 3f).

The microbial community structure revealed by metagenomics sequencing exhibited substantial concordance with 16S rRNA gene sequencing-based results at both phylum and family taxonomic levels (Fig. 3c, Fig. 3g and Table S3). In terms of relative gene abundance, Proteobacteria occupied the highest proportion of 60.6% and Thaumarchaeota 11.6%, followed by Bacteroidetes (7.4%), Actinobacteria (5.8%), Verrucomicrobia (2.9%), Euryarchaeota (2.6%), Nitrospina (1.3%), Nitrotoga (1.3%), and Cyanobacteria (1.3%; Fig. 3c) in water column. Vertically, the relative abundance of chemolithoautotrophic microorganisms represented by Thaumarchaeota and Euryarchaeota increased by 8.9% and 3.7% from surface to bottom water, respectively (Fig. c), accompanied by elevated gene abundances in nitrite oxidizers (Nitrospina and Nitrotoga) and heterotrophic Verrucomicrobia (Fig. 3c). On the contrary, the gene abundance for Cyanobacteria exhibited a 2.3% of reduction in oxygen-depleted bottom layer, while Proteobacteria decreased by 13.0% (Fig. 3c), with Rhodobacteraceae, Rhodospirillaceae, and Halieaceae declining by 3.2%, 1.2%, and 2.9%, respectively (Fig. 3g). Similarly, the gene abundance of Bacteroidetes including Flavobacteriaceae and Cryomorphaceae also presented a decrease trend (Fig. 3g). Notably, the Thaumarchaeota enrichment in the oxygen-depleted water included not only the cultured Nitrososphaeraceae but also an uncultivated Thaumarchaeota clade (named Thaumarchaeota_norank), which exhibited an average abundance of 4.0% and increased by 5.9% in bottom waters (Fig. 3g).

According to metaproteomic analysis, the total protein expression signals of microbial communities were higher in surface waters than those in bottom waters (Fig. 3d, Fig. 3h and Table S3). At the phylum level, Proteobacteria, Thaumarchaeota, Cyanobacteria, Actinobacteria, and Bacteroidetes exhibited substantial protein expressions, accounting for 12.5%, 1.2%, 2.3%, 0.8%, and 0.5% of total protein signals in surface waters, whereas their proportions in bottom waters constituted 13.8%, 3.4%, 0.8%, 0.9%, and 0.5%, respectively (Fig. 3d). At the family level, Thaumarchaeota, Cyanobacteria, and Bacteroidetes primarily expressed proteins in Nitrososphaeraceae, GpIIa, and Flavobacteriaceae, respectively. Whereas Proteobacterial expression predominantly occurred in Pelagibacteraceae, Rhodobacteraceae, and Alteromonadaceae (Fig. 3h). Vertical structural variations revealed differential protein expression patterns, most notably in Thaumarchaeota and Nitrospinae, which showed 2.8-fold and 3.3-fold increases of expression intensity proportion in bottom low oxygen waters compared to those in surface oxygen-rich layer (Fig. 3d). While Cyanobacteria showed a 2.9-fold decrease in

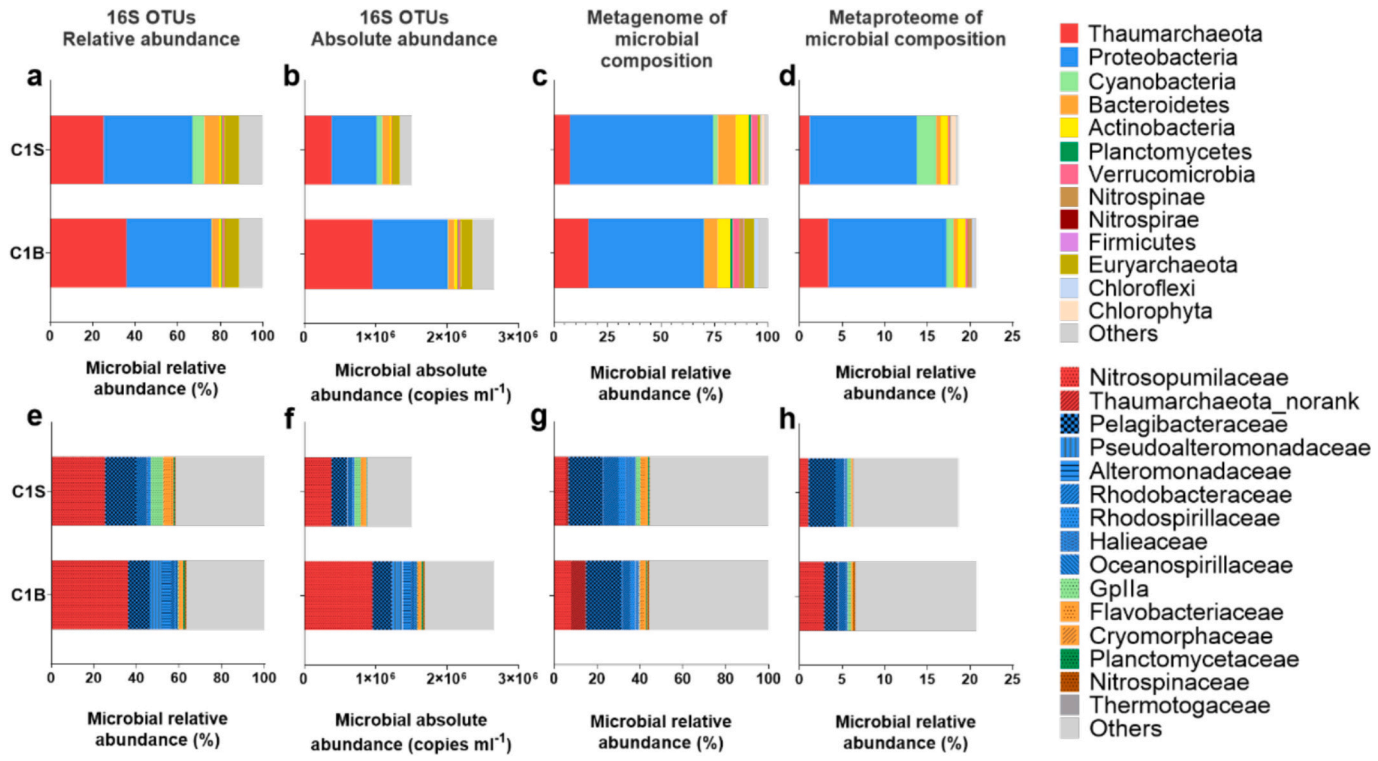


Fig. 3. The composition of microbial community based on 16S rRNA gene sequencing and meta-omics in surface (C1S) and bottom water (C1B) at (a-d) phylum and (e-h) family taxonomic levels.

bottom water (Fig. 3d).

3.3. The distribution of functional genes and proteins related to nitrogen and sulfur metabolisms

Through metagenomic analysis of metabolic functional genes in surface and bottom seawater, a total of 192 million reads were detected, which were assembled into 1.16 million contigs (Table S4). This yielded 2.26 million predicted open reading frames (ORFs), with a total sequence length of 1.285 billion bp and an average length of 570.91 bp (Table S1). Functional classification based on COG categories revealed that microbial functional genes were predominantly distributed within

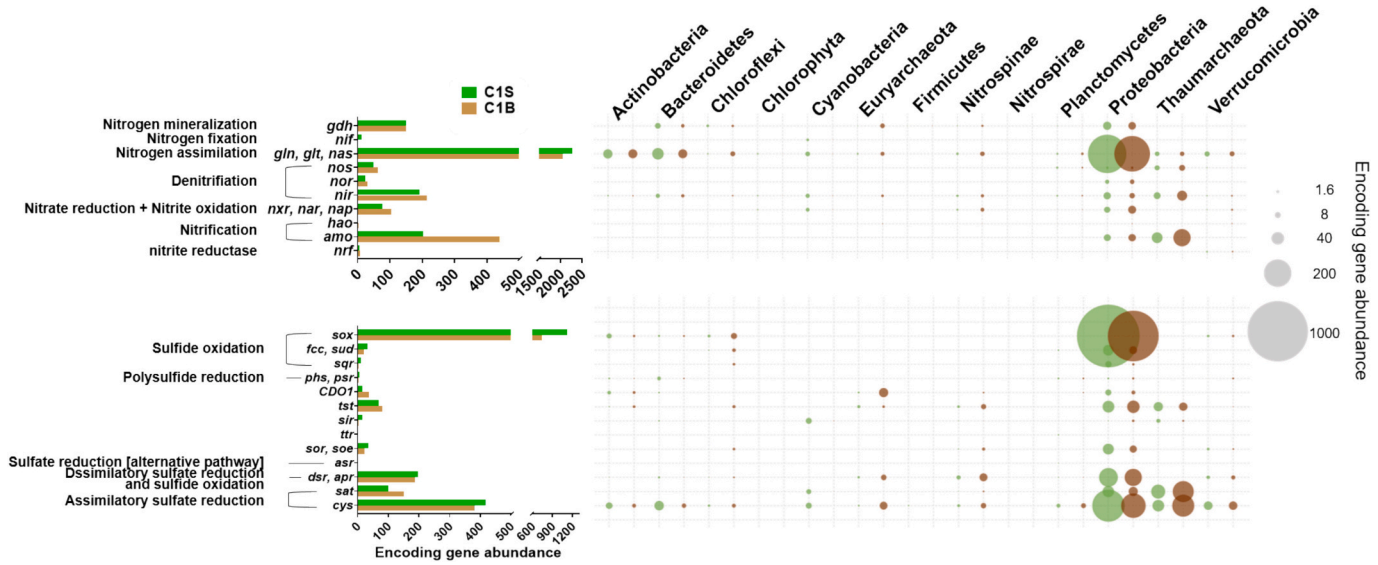


Fig. 4. The abundance of metabolic genes in nitrogen and sulfur pathways and the dominant microbial communities in hypoxic region of East China Sea. *gdh*, NADP-specific glutamate dehydrogenase; *nif*, nitrogen fixation; *gln*, *glt*, *nas*, glutamine synthetase; *nos*, nitrous-oxide reductase; *nor*, nitric oxide reductase; *nir*, ferredoxin–nitrite reductase; *nxr*, *nar*, *nap*, nitrite oxidoreductase; *hao*, hydroxylamine oxidoreductase; *amo*, ammonia monooxygenase; *nrf*, nitrite reductase by formate; *sox*, sulfur-oxidizing protein; *fcc*, sud, sulfide dehydrogenase; *sqr*, sulfide quinone oxidoreductase; *phs*, psr, thiosulfate reductase; *CDO1*, cysteine dioxygenase; *tst*, thiosulfate/3-mercaptopyruvate sulfurtransferase; *sir*, sulfite reductase (ferredoxin); *ttr*, tetrathionate reductase; *sor*, *soe*, sulfite dehydrogenase; *asr*, anaerobic sulfite reductase; *dsr*, sulfite reductase; *apr*, adenylylsulfate reductase; *cysJ*, *cysI*, sulfite reductase (NADPH); *cysC*, *cysN*, *cysNC*, *cysD*, adenylylsulfate kinase; *sat*, sulfate adenylyltransferase.

"Amino acid transport and metabolism" and "Energy production and conversion" classifications (Fig. S1).

Our microbial metaproteomic analysis obtained approximately 120 thousand mass spectrometry spectra, yielding matches to roughly 15 thousand peptide sequences (Table S5). Among these, 11,363 unique peptides were identified, collectively corresponding to 6302 protein groups. Subsequently, 1505 proteins were successfully quantified (Table S2). Analysis of COG functional categories revealed that microbial protein expression in the hypoxic waters of the East China Sea was predominantly associated with "Inorganic ion transport and metabolism (326 proteins)" and "Amino acid transport and metabolism (267 proteins)" (Fig. S1), indicating inorganic ions and organic nitrogen, particularly amino acid compounds, serve as primary metabolic substrates for microorganisms in this environment.

Nitrogen is redox sensitive, the interconversion pathways among diverse forms provide unique indicators of microbial biogeochemical responses oxygen variations. Sulfate is the most abundant electron acceptor, which drives the coupled biogeochemical transformations of multi elements in hypoxic environments. Thus, we analyzed the distribution of key functional genes (Fig. 4) and their corresponding protein expression (Fig. 5) in relation to nitrogen and sulfur metabolic pathways across the oxygen gradient in the Yangtze River Estuary. Regarding to nitrogen metabolism, the highest abundance of enzymes encoding gene was nitrogen assimilation, including glutamate synthase (*gltBDS*), assimilatory nitrate reductase (*nasA*), and glutamine synthetase (*glnAB*), which was primarily mediated by Proteobacteria, Bacteroidetes, and Actinobacteria (Fig. 4). Nitrification represented another major nitrogen metabolic pathway, which was mediated mainly by Thaumarchaeota, with their ammonia monooxygenase (*amo*) genes exhibiting higher abundance in bottom low oxygen waters (Fig. 4). In addition, the nitrogen reduction related enzymes encoding genes, such as nitrate reductases (*nar* and *nap*), nitrite reductases (*nir* and *nrf*), nitric oxide reductase (*norB*), and nitrous oxide synthase (*nos*), were widely distributed in both surface and bottom waters, with Proteobacteria and Thaumarchaeota identified as the primary gene carriers (Fig. 4). Notably, Thaumarchaeota showed the highest abundance of *nir* gene in bottom waters (Fig. 4). Additionally, microbial communities exhibited comparable encoding gene abundance with regard to nitrogen mineralization processes regardless of water layers (Fig. 4).

According to metaproteomic results, nitrogen metabolism-related protein expression primarily involved in nitrogen assimilation, nitrification, and partial denitrification processes (Fig. 5a and b). Among them, Cyanobacteria and Thaumarchaeota both expressed abundant nitrogen uptake-associated proteins, including citrate synthase (GltA), glutamate synthase (GltBD), glutamine synthetase (GlnAB), nitrogen regulatory protein P-II (GlnBK), and ammonium transporters (AMT), with significant higher expression in the oxygenated surface waters (Fig. 5a and b). Nitrification activity was evident, with ammonia monooxygenase (AmoABC) proteins primarily detected in Thaumarchaeota, while nitrite oxidoreductase (NxrAB) proteins are predominantly expressed by Nitrospina (Fig. 5a and b). For nitrogen reduction pathways, while metagenomic data revealed the full genetic potential across microbial lineages, the metaproteomic profile specifically indicated a substantial expression of nitrite reductase (NirK) proteins in Thaumarchaeota, alongside moderate nitrate reductase (NarGZ) protein detection in Nitrospinae (Fig. 5a and b). Notably, no other denitrification-related proteins were detected (Fig. 5a and b). These protein expression signals collectively suggested an enhancement of nitrification and partial denitrification pathways within the underlying low-oxygen waters (Fig. 5c).

For sulfur metabolism, encoding genes associated with sulfur oxidation and assimilatory/dissimilatory sulfate reduction pathways were detected in the study region (Fig. 4). Proteobacteria and Thaumarchaeota were the primary microbial groups mediating these sulfur metabolic processes, with Proteobacteria dominated in surface waters, while Thaumarchaeota additionally served as significant contributors to both assimilatory and dissimilatory sulfate reduction in bottom low oxygen waters. In addition, Thaumarchaeota also presented encoding

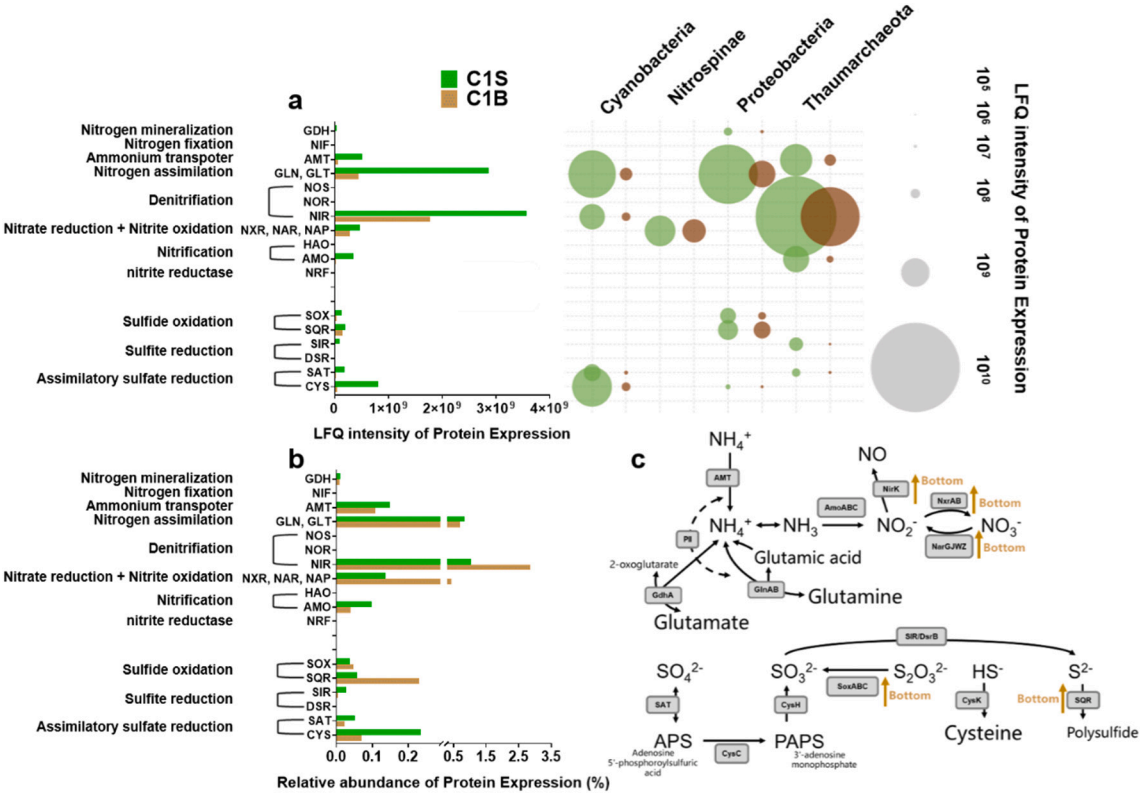


Fig. 5. Expression characteristics of protein involved in microbial nitrogen and sulfur metabolisms in hypoxic region of East China Sea.

genes with respect to thiosulfate/3-mercaptopyruvate sulfurtransferase (*tst*) and ferredoxin-dependent sulfite reductase (*sir*) (Fig. 4). Protein expression related to sulfur metabolism was primarily localized to sulfur oxidation and assimilatory sulfate reduction processes (Fig. 5a and b). The sulfur oxidation proteins, including sulfur oxidation multienzyme complex SoxABC and sulfide oxidoreductase (SQR), were predominantly expressed within Proteobacteria (Fig. 5a). Additionally, Cyanobacteria primarily expressed proteins essential for assimilatory sulfate reduction, such as sulfate adenylyltransferase (SAT), adenylylsulfate kinase (CysC), phosphoadenosine phosphosulfate reductase (CysH), and cysteine synthase (CysK). Despite genomic evidences have indicated a strong potential for assimilatory sulfate reduction in Thaumarchaeota, no related proteins were detected in the water column (Fig. 5a and b). Nearly all sulfur metabolism-related proteins exhibited peak expression levels in surface oxygenated waters, while the relative abundance of proteins involved in sulfur oxidation pathways, specifically SOX and SQR, increased in the bottom hypoxic waters (Fig. 5b and c).

3.4. The gene abundance and protein expression of main transporters

Analysis of microbial transporter gene abundances associated with carbon and nitrogen metabolism in East China Sea (Table S6) revealed distinct distribution patterns for ABC transporters, TonB-dependent transporters, and dissolved organic nitrogen (DON) transporters. Proteobacteria consistently exhibited the highest gene abundances for all three transporter types across the water depth, with universally higher gene abundances in surface waters (Fig. 6). Specifically, the carbohydrate transporters encoding genes were predominantly associated with ABC transporters, with minor contributions from TonB transporters. ABC transporter genes were ubiquitously detected across dominant microbial taxa, with Proteobacteria displaying the highest gene abundance particularly in surface water, followed by Actinobacteria and Thaumarchaeota (Fig. 6). In contrast, TonB transporter genes were exclusively identified in Bacteroidetes and Proteobacteria, with consistent higher abundance in surface waters (Fig. 6). Regarding to DON transporter encoding genes, high abundances were observed in Proteobacteria, Thaumarchaeota, Bacteroidetes, Actinobacteria, and Cyanobacteria, primarily facilitating the transport of amino acids, peptides, nucleic acid derivatives, vitamins, polyamines, and other nitrogen-rich organic compounds (Fig. 6). Concomitant with increasing depth and decreasing DO concentration, DON transporter gene abundances declined in Proteobacteria, Bacteroidetes, and Actinobacteria within the bottom low oxygen waters, while corresponding increases were observed in Thaumarchaeota, Euryarchaeota, Chloroflexi, and Nitrospinae (Fig. 6).

Based on our metaproteomic results (Table S7), microbial taxa expressing ABC transporter proteins primarily included Actinobacteria, Chloroflexi, Cyanobacteria, and Proteobacteria, all presenting consistent vertical distribution patterns with relative higher protein expression in surface waters compared to bottom low oxygen layers (Fig. 6). TonB transporter-encoding gene expression was primarily identified in Bacteroidetes and Proteobacteria, also exhibiting elevated levels in surface waters (Fig. 6). Similarly, DON transporter protein expression involved analogous microbial groups and vertical trends as observed for ABC transporters (Fig. 6). Integrating transporter gene abundance and protein expression, higher gene abundance within the same microbial group (e.g., Proteobacteria) generally corresponded to increased protein expression (Fig. 6). However, no absolute correlation existed across different taxa, for example, the expression of transporter was dominated by organic nitrogen transporters for amino acids and peptides, along with carbohydrate ABC transporters (Fig. 6). Although genes encoding nucleoside/nucleotide transporters, polyamine transporters, and other

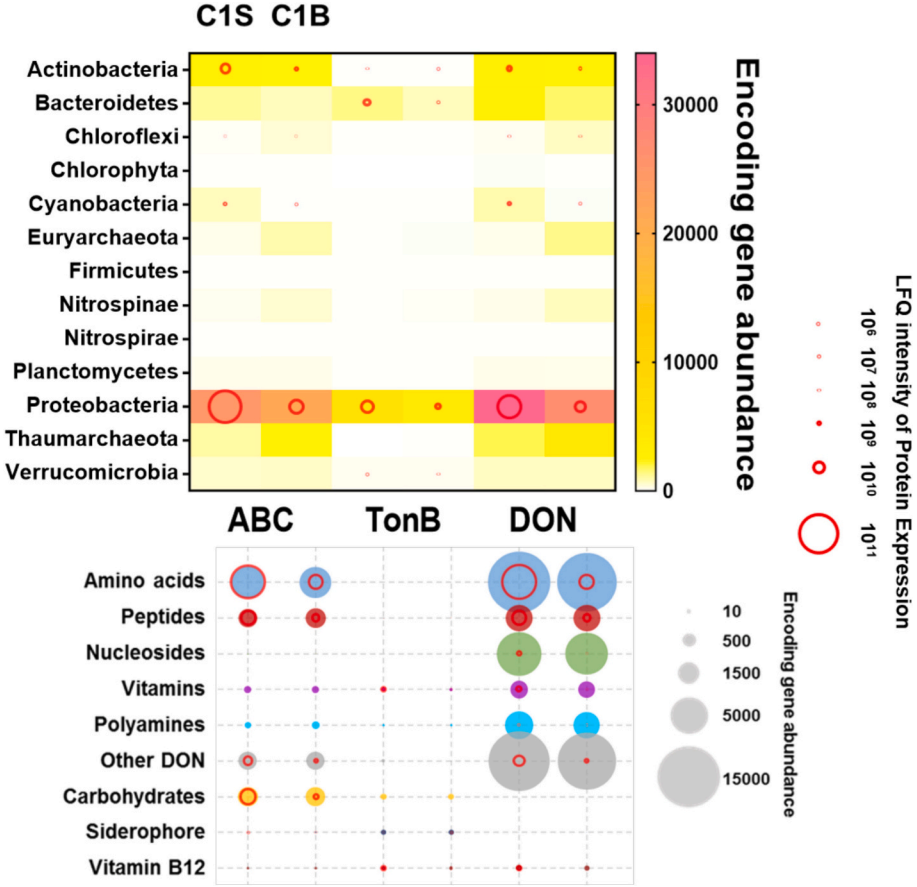


Fig. 6. The distribution of gene abundance and protein expression of main transporters in hypoxic region of East China Sea.

DON transporters exhibit higher abundance, while the expression levels of corresponding proteins were significantly lower (Fig. 6).

In addition, we assembled 7 high-quality archaeal metagenome-assembled genomes (MAGs) with completeness >50% and contamination <3%, including four Thaumarchaeota MAGs and three Euryarchaeota MAGs (Table 2). Among the four Thaumarchaeota, two *Nitrosopumilus* strains were identified, such as C1B.bins.66 (*Nitrosopumilus* sp003702465), the most abundant strain (2.02% of relative abundance; Table 2), and C1S.bins.88 with 76.21% completeness (Table 2). Meanwhile, two *Nitrosopelagicus* strains were recovered. The Euryarchaeotal MAGs are comprised of MGIIb-O2, Thalassarchaeum, and MGIIb-O5 (Table 2). The analysis of core functional genes revealed that the 4 Thaumarchaeota MAGs encode nitrogen-cycling core genes (*amo*, *nirK*, *amt*, *glnAK*), collectively forming the key functional module for nitrification, partial denitrification, nitrogen transport and mineralization (Table S8). The 3 MGII Euryarchaeota MAGs predominantly carry dissimilatory sulfur metabolism genes (*cysCHJN*, *dsrA*, *CDO1*), alongside encoding genes of carbohydrate-active enzymes families (GT4) and peptidases families (M24, M32, M50) (Table S8).

4. Discussion

The formation of seasonal hypoxic zone in the East China Sea off the Yangtze River Estuary arises from synergistic interactions multiple environmental drivers. The high nutrient inputs from the Changjiang Diluted Water (Table 1) stimulate summer phytoplankton blooms in surface waters (Fig. 2c). Subsequently, the sedimentation and microbial decomposition of algae-derived organic matter substantially intensify oxygen consumption in bottom waters (Chen et al., 2021; Dalseno et al., 2024; Zhang et al., 2021; Zhou et al., 2020). In addition, the topographic restricts horizontal exchange of bottom waters while vertical mixing is impeded by persistent stratification, critically limiting oxygen ventilation (Wang et al., 2022). Crucially, sediment resuspension (Fig. 2f) introduces reduced chemical species (e.g., Fe^{2+}, Mn^{2+}) and organic matter from anoxic benthic layers into the oxygenated water column. This process intensifies oxygen consumption by stimulating aerobic respiration, ultimately expanding the hypoxic zone (Lin et al., 2025). However, the weak water column stratification (Fig. 1) and a minimum DO concentration of 3.2 mg/L (Table 1) during our sampling period collectively indicate that the hypoxic zone in the Yangtze River Estuary was still in a

Table 2
Summary of metagenomic assembly genomes of archaea from hypoxic region, East China Sea, with the blast results in transcripts from Bohai Sea (Han et al., 2022).

#Bin Id	Bin size (Mbp)	Mapped reads[a]	Completeness[b]	Contamination[c]	Classification	% homologous reads (metagenome in East China Sea)[d]	% homologous reads (metatranscriptome in Bohai)[e]	% homologous reads(A45-B FL in Bohai)[f]
C1S.bins.88	1.02	311,570	76.21	0	d_Archaea; p_Thaumarchaeota; c_Nitrososphaeria; o_Nitrososphaerales; f_Nitrosopumilaceae; g_*Nitrosopumilus*	0.42	0.03	0.09
C1B.bins.66	0.71	1,492,528	53.63	1.29	d_Archaea; p_Thaumarchaeota; c_Nitrososphaeria; o_Nitrososphaerales; f_Nitrosopumilaceae; g_*Nitrosopumilus*; s_*Nitrosopumilus* sp003702465	2.02	0.17	0.66
C1B.bins.31	0.55	385,381	53.07	2.91	d_Archaea; p_Thaumarchaeota; c_Nitrososphaeria; o_Nitrososphaerales; f_Nitrosopumilaceae; g_*Nitrosopelagicus*; s_*Nitrosopelagicus* sp902552015	0.68	0.003	0.01
C1S.bins.34	0.84	51,254	52.15	0.97	d_Archaea; p_Thaumarchaeota; c_Nitrososphaeria; o_Nitrososphaerales; f_Nitrosopumilaceae; g_*Nitrosopelagicus*	0.15	0.01	0.05
C1B.bins.49	1.33	189,915	77.25	0	d_Archaea; p_Thermoplasmatota; c_Poseidoniia_A; o_Poseidoniales; f_Thalassarchaeaceae; g_MGIIb-O2; s_MGIIb-O2 sp002686525	0.20	0.003	0.01
C1B.bins.27	1.36	103,116	77.94	1.87	d_Archaea; p_Thermoplasmatota; c_Poseidoniia_A; o_Poseidoniales; f_Thalassarchaeaceae; g_*Thalassarchaeum*; s_*Thalassarchaeum* sp002501885	0.11	1.23E-05	4.77E-05
C1B.bins.41	1.08	54,169	64.63	2.53	d_Archaea; p_Thermoplasmatota; c_Poseidoniia_A; o_Poseidoniales; f_Thalassarchaeaceae; g_MGIIb-O5; s_MGIIb-O5 sp002504435	0.06	5.33E-06	0

[a] Compares the number of reads belonging to bin Contigs;
[b] Integrity, which estimates the integrity of the genome from information about the presence/absence of marker genes and the expected co-occurrence of those genes, the greater the value, the better;
[c] The contamination degree, estimated from the occurrence of multi-copy marker genes and the expected co-occurrence information of these genes, the smaller the value, the better;
[d] Target Number of reads in Zhoushan DNA-seq set/total number of reads in Zhoushan macro gene sequence set;
[e] Target Number of reads in the Bohai Sea macrotranscriptome sequence set/total number of reads in the Bohai Sea macrotranscriptome sequence set (Han et al., 2022);
[f] Objective to compare all bin ORF sequences to the number of reads in the Bohai Sea A45 bottom water RNA-seq collection and the total number of reads in the Bohai Sea macro transcriptome sequence collection (Han et al., 2022).

developing phase, not yet reaching peak intensity.

Integrated analyses of microbial community composition, metagenomics, and metaproteomics reveal that the community structure and metabolic processes of dominant microorganisms in the East China Sea are primarily governed by dissolved inorganic nitrogen (DIN) concentration, DO levels, and sediment resuspension. Vertically, pronounced gradients in redox conditions and particulate turbidity collectively drive microbial niche differentiation and metabolic shifts (Fig. 3–5). In surface layer, abundant nutrient loads from the Changjiang Diluted Water establish a phytoplankton-dominated photoautotrophic community, co-occurring with opportunistic heterotrophic bacteria. Key functional groups include Flavobacteriia utilizing high-molecular-weight carbohydrates (Teeling et al., 2012), Pelagibacterales taxa preferentially assimilating low-molecular-weight organic nitrogen, and Roseobacter-group members (e.g., Rhodobacter and Rhodovulum) with multiple nitrogen metabolic pathways (Zheng et al., 2020). This assemblage was highly similar to microbial signatures characteristic of algal bloom ecosystems (Han et al., 2022). Coupled with our field hydrochemical data (Fig. 2 and Table 1), these findings indicated that the study area was likely undergoing a critical successional phase of phytoplankton bloom development during the observation period. In addition to oxygen gradients and sediment resuspension, light availability serves as another critical factor governing the vertical structure of microbial communities and their mediated carbon-nitrogen cycling processes (Zhang et al., 2024b). In sunlit surface waters, high light condition promotes photoautotrophic carbon fixation by phytoplankton while simultaneously suppressing the metabolism of nitrifying microorganisms such as Thaumarchaeota (Wan et al., 2021). Consequently, Thaumarchaeota predominantly inhabit aphotic bottom environments mediating active nitrification process (Bergauer et al., 2025).

Multi-omics analyses reveal that the microbial community in bottom water with low DO exhibits typical hypoxia-adaptation features (Fig. 3–5 and Table S3). Synergistic effects of low DO and high suspended particulate matter shape a chemolithoautotroph-dominated assemblage, including Thaumarchaeota, nitrite-oxidizing bacteria (Nitrospina, Nitrospira, Nitrospinae), and facultative anaerobes (such as Planctomycetes and MGII Euryarchaeota), and Proteobacterial genera (Pseudomonas, Alteromonas). Such community structure demonstrates high conservation with observations from global hypoxic systems (Liu et al., 2024) and permanent oxygen minimum zones (Beman et al., 2021; Guo et al., 2022; Li et al., 2024), suggesting universal ecological strategies for these microbes in marine deoxygenation environments. Crucially, the unique environmental features of the hypoxic zone in the Yangtze River Estuary significantly shape its microbial community composition. For instance, sediment resuspension promotes the proliferation of specific microbial taxa adapted to a particle-attached lifestyle, inculding Thaumarchaeota, MGII Euryarchaeota, Planctomycetes, and Proteobacteria (Huanca-Valenzuela et al., 2025; Karthäuser et al., 2021). Specifically, suspended particles can provide substrate ammonium and serve as microenvironments against photodamage for Thaumarchaeota (Proctor et al., 2023). In contrast, the other three groups exhibit a competitive advantage in these high-turbidity bottom waters due to their metabolic preference for utilizing high-molecular-weight organic compounds (Farkas et al., 2023; Xie et al., 2018).

The microbial nitrogen metabolism in East China Sea coastal waters exhibits a significant vertical variation driven by redox gradients, with community structural differences directly governing selective activation of nitrogen transformation pathways. In oxygen-replete surface layer, photoautotrophs preferentially assimilate DIN such as NO_3^--N and NH_4^+-N, via highly expressed nitrogen assimilation genes, while concurrent upregulation of DON transporters in aerobic microbes, particularly for amino acid uptake and metabolism (Fig. 6), confirms organic nitrogen assimilation as another nitrogen source. By contrast, microbes in the bottom low oxygen water show a typical chemolithoautotrophic metabolism (Figs. 4 and 5). Although metagenomic analyses detected complete genetic modules for nitrogen reduction (Fig. 4 and Table S4), including denitrification genes (nar/nap, nir, nor, and nos) and dissimilatory nitrate reduction to ammonium (DNRA; nir/nrf), our metaproteomics only reveal a significant expression of nitrate reductases (NAR, NAP and NIR; Fig. 5 and Table S5). This decoupling between genomic potential and proteomic expression of denitrification pathway is largely stem from the limitations of high oxygen concentration and low substrates. On one hand, the ambient oxygen conditions have not yet reached the critical threshold required to activate downstream enzymes (e.g., nor and nos), despite the presence of nar/nap and nir genes. Previous studies have suggested that partial denitrification to N_2O can occur at higher oxygen levels compared to complete denitrification to N_2 (Pascal et al., 2025; Tang et al., 2025). The critical oxygen threshold for complete denitrification is system-specific, but our results are consistent with observations in other coastal systems where nor and nos expression are suppressed above ~32–59 mg/L of DO (Pascal et al., 2025; Tang et al., 2025). On the other hand, the low concentration of nitrite in the water column (Table 1) implies that nitrite availability, rather than solely oxygen, is also a limiting factor for complete denitrification. Overall, this vertical differentiation of nitrogen-cycling functional genes (e.g., nitrogen reduction genes and DON transporters) reflects the efficient adaptation of microbial communities to low oxygen conditions, reshaping nitrogen cycling pathways across oxygen gradients, and serves as a critical molecular marker for assessing the ecological functional state of hypoxic zones and predicting their responses to global change.

Both metagenomic and metaproteomics indicated ubiquitous distribution of Thaumarchaeota throughout the water column, with significantly higher abundances in hypoxic bottom waters (Fig. 4, Fig. 5 and Table S3). Previous studies have suggested that ammonium concentration exerts predominant regulatory control over the growth and niche partitioning of Thaumarchaeota (Dai et al., 2022; Qin et al., 2024; Stahl and De La Torre, 2012). The ammonium derived from Changjiang Diluted Water inputs and sediment resuspension (Fig. 2 and Table 1) directly maintain their colonization in the whole water column. As key drivers of nitrification, Thaumarchaeota harbor high-abundance *amoA* genes encoding ammonia monooxygenase (Fig. 4), the detection of expressed AMO proteins (Fig. 5) functionally validates active nitrification in both water layers. However, the significant increase in ammonia-oxidizing gene abundance in hypoxic waters suggests that Thaumarchaeota may hold a greater nitrification potential in aphotic bottom environments, possibly due to reduced photo-inhibition and decreased competition with phytoplankton (Wan et al., 2021).

Metagenomic results identify that *Nitrosopumilus* (strains C1B.bins.66, *Nitrosopumilus* sp003702465; Table 2 and Table S3) is the predominant Thaumarchaeotal ecotype in hypoxic waters of East China Sea, aligning with global observations of deoxygenated marine systems. Regionally, this genus overwhelmingly dominates Thaumarchaeotal assemblages in China's marginal seas, including the Pearl River Estuary (Xie et al., 2018), Jiulong River Estuary (Guo et al., 2018), and Bohai Sea (Han et al., 2022), where it constitutes up to 99% of Thaumarchaeotal populations in certain estuarine zones (Zou et al., 2020). Globally, active *Nitrosopumilus* populations persist in the Gulf of Mexico (Gillies et al., 2015) and oceanic oxygen minimum zones (Glass et al., 2020; Ren and Wang, 2022). The experimental work has demonstrated that *Nitrosopumilus maritimus* can produce oxygen under hypoxic conditions to support its own ammonia oxidation (Kraft et al., 2022). This capability provides a key mechanism to explain the widespread presence of ammonia-oxidizing Thaumarchaeota in marine oxygen minimum zones. Simultaneously, Qin et al. (2024) revealed distinct metabolic preferences among different lineages of ammonia oxidizers. For instance, *Nitrosopumilus piranensis* D3C preferentially utilizes ammonia over urea, while β-ammonia-oxidizing bacteria favor urea utilization. Such niche differentiation effectively avoids direct competition for ammonium among different microbial groups. Taken together, the unique conditions in the Yangtze River Estuary (high nutrient input and intense sediment resuspension) were favorable for the proliferation of

Thaumarchaeota, particularly *Nitrosopumilus* species. High nutrient input primarily affects *Nitrosopumilus* indirectly by stimulating phytoplankton blooms in surface waters, promoting the sinking and degradation of organic particles, accelerating the formation of hypoxic zones in bottom waters, and enhancing ammonium regeneration, thereby creating favorable conditions for growth of *Nitrosopumilus*. Meanwhile, intense sediment resuspension creates a dynamic and particle-rich environment in bottom water, providing additional ammonium source and particulate habitats for *Nitrosopumilus*. The ability of *Nitrosopumilus* to survive on particles can further enhance its nutrient acquisition and reduce competition with free-living ammonia-oxidizing bacteria (Han et al., 2022). Additionally, *Nitrosopumilus* possesses broad-salinity adaptation ability (Qin et al., 2017), giving it a competitive advantage over ammonia-oxidizing bacteria and other types of ammonia-oxidizing archaea (such as *Nitrosopelagicus* spp. and *Nitrosarchaeum* spp.) in estuarine environments.

From a physio-ecological perspective, Thaumarchaeota develop multiply strategies to adapt hypoxia stress. At the substrate acquisition level, their ammonia monooxygenase system exhibits high affinity for ammonium with half saturation constant values as low as 10–100 nM, enabling metabolic maintenance and competitive dominance under oligotrophic conditions (Santoferrara et al., 2022; Straka et al., 2019; Wolf et al., 2025). For energy conservation, these archaea optimize electron transfer efficiency under oxygen limitation by upregulating cytochrome *c* oxidases (Murali et al., 2024), while coordinated antioxidant enzyme systems mitigate reactive oxygen species damage (Han et al., 2022). Notably, their nitrogen metabolic plasticity extends beyond ammonia oxidation, the urea hydrolysis pathways provide additional ammonium sources (Stein, 2019), and nirK gene induction under ammonium limitation condition potentially activates nitrite reduction pathway (Reyes et al., 2020). Meanwhile, Thaumarchaeota rely on the iron-sulfur cluster proteins during ammonia oxidation (Diamond et al., 2022), which increases their iron demand and thus explains the observed high expression of iron ion transport and metabolic-related proteins in the bottom waters (Fig. S1). In addition, historical studies have found that dissolved iron concentrations in bottom hypoxic waters (12.4–26.7 nmol L^{-1}) off the Yangtze River Estuary were 2–3 times higher than that in surface waters (4.5–13.2 nmol L^{-1}; Zhang et al., 2022). The higher iron concentration satisfies the iron demand of Thaumarchaeota, thereby further supporting their thriving in low-oxygen waters. Furthermore, quorum sensing mediated biofilm formation enhances environmental resilience, with horizontal gene transfer within aggregates accelerating adaptive evolution (Huang et al., 2022; Liu et al., 2024).

Thaumarchaeota-mediated ammonia oxidation acts as a critical component of nitrification, driving the conversion of reduced nitrogen to oxidized forms and their fluxes in marine systems (Pajares and Pelayo, 2025). Meanwhile, their metabolic byproduct nitrite serves as the essential substrate for both nitrite oxidizers and denitrification communities, collectively determining the removal flux of reactive nitrogen (Hernández-Magaña and Kraft, 2024; Martens-Habbena and Qin, 2022). Furthermore, Thaumarchaeota participate in marine carbon cycle through their chemolithoautotrophic 3-hydroxypropionate/4-hydroxybutyrate (HP/HD) cycle-mediated dark carbon fixation process (Martens-Habbena and Qin, 2022). Recent observational data from Bayer et al. indicate that Thaumarchaeota-mediated ammonia oxidation averagely contributes 4–25% of the total dark carbon fixation in the eastern tropical Pacific, and can even exceed 50% particularly in the upper oxygen-deficient zone (Bayer et al., 2025). In the Yangtze River Estuary, the total dark carbon fixation rate in surface waters ranged from 0.02 to 1.44 μmol C L^{-1} h^{-1}, with a minor contribution (0.3–4.0%) from Thaumarchaeota (Cui et al., 2025), while it is likely to increase in the bottom low oxygen waters where Thaumarchaeota were concentrated. Given the ecological preference for oligotrophic marine environments, their contribution to dark carbon fixation is generally higher in open ocean than that in coastal areas. Nevertheless, both metaproteomic and rate data consistently suggest that Thaumarchaeota serve as one of the contributors to carbon sequestration in the dark ocean.

Coastal hypoxic zones typically exhibit pronounced spatiotemporal variabilities in hypoxia extent and microbial community composition due to seasonal river discharge, wind-driven mixing, and nutrient inputs (Sheng et al., 2024; Zhang et al., 2023). Previous studies have shown that under the regulation of environmental factors such as temperature, light, dissolved oxygen, and nutrients, Thaumarchaeota present seasonal and regional shifts in abundance and activity (Liu et al., 2018; Zou et al., 2022). Their abundance and ammonia oxidation rates often peak during mid-summer and in hypoxia transition zones (Hollibaugh et al., 2014), and were significantly higher during hypoxia peak periods compared to hypoxia development phases (Santoferrara et al., 2022). These findings suggest that our observed patterns may represent an early adaptive strategy of Thaumarchaeota to incipient hypoxia, while seasonal changes and more extreme hypoxic conditions may further select for alternative functional adaptations. Our study focused on a single site during the developing phase of hypoxia in the Yangtze River Estuary, which limits our ability to generalize findings to peak hypoxia or non-hypoxic periods and areas. However, this phase is ecologically significant because it represents the initial transition from oxic to anoxic conditions, during which microbial communities must rapidly adapt to declining oxygen levels. Under the context of projected marine deoxygenation, future studies should integrate muti-seasonal sampling and multi-station transects to assess how microbial communities, particularly Thaumarchaeota, adapt to varying degrees of hypoxia and nutrient availability across greater spatial and temporal scales.

5. Conclusions

This integrated multi-omics study reveals a redox-driven niche partitioning of microbial communities during the developing phase of hypoxia in Yangtze River Estuary, with surface oxic waters dominated by photoautotrophic phytoplankton and heterotrophic bacteria, while low-oxygen bottom layers enriched chemolithoautotrophs and particle-attached facultative anaerobes. Accompanying this structural shift was a functional transition in nitrogen metabolism from assimilation in surface waters to active nitrification coupled with partial nitrate/nitrite reduction in bottom waters. The genomic potential for complete denitrification was present across the microbial community, however, metaproteomic evidence showed only the significant expression of nitrate and nitrite reductases. This decoupling between genomic capacity and proteomic expression underscores a state of genomic preparedness and metabolic plasticity, indicating that ambient oxygen levels remained above the threshold for activating the full denitrification pathway. Thaumarchaeota, particularly *Nitrosopumilus* strains, emerged as keystone taxa in bottom low oxygen waters, driving nitrification and dark carbon fixation, thereby acting as a key coupler of nitrogen and carbon biogeochemical cycles in the developing hypoxic zone. These findings highlight the adaptive strategies of key microbial taxa to deoxygenation stress and provide predictive insights into microbial-mediated biogeochemical feedbacks under expanding coastal hypoxia.

CRediT authorship contribution statement

Yu Han: Methodology, Investigation, Formal analysis, Writing – review & editing, Writing – original draft. **Le Liu:** Methodology, Investigation. **Quanrui Chen:** Resources, Investigation. **Wei Fan:** Project administration, Funding acquisition. **Kai Tang:** Resources, Project administration, Funding acquisition. **Ehui Tan:** Writing – review & editing. **Zhijie Zhang:** Writing – original draft. **Airui Wang:** Writing – original draft.

Declaration of competing interest

The authors declare that they have no known competing financial

interests or personal relationships that could have appeared to influence the work reported in this paper.

Acknowledgements

This study was supported by the National Natural Science Foundation of China (#42188102, #42306120, and #42076160); Hainan Provincial Natural Science Foundation of China (#425RC695); and the Ministry of Science and Technology (MOST) ONCE project. We are grateful to anonymous reviewers for their constructive comments. The data that support the findings of this study are available on request from the corresponding author.

Appendix A. Supplementary data

Supplementary data to this article can be found online at https://doi.org/10.1016/j.marpolbul.2026.119293.

Data availability

Data will be made available on request.

References

Avrahami, Y., Siano, R., Rubin-Blum, M., Koplovitz, G., Henry, N., De Vargas, C., Frada, M.J., 2025. Seasonal transition in the dominance of photoautotrophic and heterotrophic protists in the photic layer of a subtropical marine ecosystem. Environ. Microbiol. Rep. 17 (4), e70126.

Bayer, B., Kitzinger, K., Paul, N.L., Albers, J.B., Saito, M.A., Wagner, M., Carlson, C.A., Santoro, A.E., 2025. Minor contribution of ammonia oxidizers to inorganic carbon fixation in the ocean. Nat. Geosci. 18, 1144–1151. https://doi.org/10.1038/s41561-025-01798-x.

Beman, J.M., Vargas, S.M., Vazquez, S., Wilson, J.M., Yu, A., Cairo, A., Perez-Coronel, E., 2021. Biogeochemistry and hydrography shape microbial community assembly and activity in the eastern tropical North Pacific Ocean oxygen minimum zone. Environ. Microbiol. 23 (6), 2765–2781.

Bergauer, K., Suffridge, C.P., Wittmers, F., Sudek, S., Giovannoni, S.J., Worden, A.Z., 2025. Dark ocean archaeal and bacterial chemoautotrophs drive vitamin B1 production in oxygen minimum zones. ISME. Communications 5 (1), ycaf077.

Bolger, A.M., Lohse, M., Usadel, B., 2014. Trimmomatic: a flexible trimmer for Illumina sequence data. Bioinformatics 30, 2114–2120. https://doi.org/10.1093/bioinformatics/btu170.

Breitburg, D., Levin, L.A., Oschlies, A., Grégoire, M., Chavez, F.P., Conley, D.J., Garçon, V., Gilbert, D., Gutiérrez, D., Isensee, K., Jacinto, G.S., Limburg, K.E., Montes, I., Naqvi, S.W.A., Pitcher, G.C., Rabalais, N.N., Roman, M.R., Rose, K.A., Seibel, B.A., Telszewski, M., Yasuhara, M., Zhang, J., 2018. Declining oxygen in the global ocean and coastal waters. Science 359, eaam7240. https://doi.org/10.1126/science.aam7240.

Chen, C.C., Shiah, F.K., Gong, G.C., Chen, T.Y., 2021. Impact of upwelling on phytoplankton blooms and hypoxia along the Chinese coast in the East China Sea. Mar. Pollut. Bull. 167, 112288.

Chen, Q., Dong, C., Li, Y., Shi, Q., Chen, X., Tang, K., Jiao, N., 2025. Shifts in microbial metabolism for algal-derived organic matter utilization under dynamic oxygen conditions. Mar. Pollut. Bull. 222, 118684.

Cui, R., Mao, T., Ping, S., Ou, Y., Dong, H., 2025. Substantial dark carbon fixation contributes to carbon sink in human-impacted estuarine and coastal waters. Anthr. Coasts 8 (1), 21.

Dai, M., Wang, L., Guo, X., Zhai, W., Li, Q., He, B., Kao, S.-J., 2008. Nitrification and inorganic nitrogen distribution in a large perturbed river/estuarine system: the Pearl River estuary, China. Biogeosciences 5, 1227–1244. https://doi.org/10.5194/bg-5-1227-2008.

Dai, X., Chen, M., Wan, X., Tan, E., Zeng, J., Chen, N., Kao, S.-J., Zhang, Y., 2022. Potential contributions of nitrifiers and denitrifiers to nitrous oxide sources and sinks in China's estuarine and coastal areas. Biogeosciences 19, 3757–3773. https://doi.org/10.5194/bg-19-3757-2022.

Dalseno, T.C., Greenwood, J., Keesing, J.K., Feng, M., 2024. Seasonal deoxygenation in a shallow coastal embayment: the role of stratification and implications for water-quality monitoring. Reg. Stud. Mar. Sci. 77, 103738. https://doi.org/10.1016/j.rsma.2024.103738.

Diamond, S., Lavy, A., Crits-Christoph, A., Matheus Carnevali, P.B., Sharrar, A., Williams, K.H., Banfield, J.F., 2022. Soils and sediments host Thermoplasmata archaea encoding novel copper membrane monooxygenases (CuMMOs). ISME J. 16 (5), 1348–1362.

Farkas, R., Mireisz, T., Toumi, M., Abbaszade, G., Sztráda, N., Tóth, E., 2023. The impact of anti-inflammatory drugs on the prokaryotic community composition and selected bacterial strains based on microcosm experiments. Microorganisms 11 (6), 1447. https://doi.org/10.3390/microorganisms11061447.

Gillies, L.E., Thrash, J.C., deRada, S., Rabalais, N.N., Mason, O.U., 2015. Archaeal enrichment in the hypoxic zone in the northern Gulf of Mexico. Environ. Microbiol. 17, 3847–3856. https://doi.org/10.1111/1462-2920.12853.

Glass, J.B., Kretz, C.B., Ganesh, S., Ranjan, P., Seston, S.L., Buck, K.N., Landing, W.M., Morton, P.L., Moffett, J.W., Giovannoni, S.J., Vergin, K.L., Stewart, F.J., 2020. Corrigendum: Meta-omic signatures of microbial metal and nitrogen cycling in marine oxygen minimum zones. Front. Microbiol. 11, 619943. https://doi.org/10.3389/fmicb.2020.619943.

Guo, R., Ma, X., Zhang, J., Liu, C., Thu, C.A., Win, T.N., Aung, N.L., Win, H.S., Naing, S., Li, H.L., Zhou, F., Wang, P., 2022. Microbial community structures and important taxa across oxygen gradients in the Andaman Sea and eastern bay of Bengal epipelagic waters. Front. Microbiol. 13, 1041521.

Guo, W., Xie, W., Li, X., Wang, P., Hu, A., Zhang, C.L., 2018. Environmental factors shaping the archaeal community structure and ether lipid distribution in a subtropic river and estuary. China. Appl. Microbiol. Biotechnol. 102, 461–474. https://doi.org/10.1007/s00253-017-8595-8.

Han, Y., Zhang, M., Chen, X., Zhai, W., Tan, E., Tang, K., 2022. Transcriptomic evidences for microbial carbon and nitrogen cycles in the deoxygenated seawaters of Bohai Sea. Environ. Int. 158, 106889. https://doi.org/10.1016/j.envint.2021.106889.

Hawley, A.K., Kheirandish, S., Mueller, A., Leung, H.T.C., Norbeck, A.D., Brewer, H.M., Pasa-Tolic, L., Hallam, S.J., 2013. Molecular tools for investigating microbial community structure and function in oxygen-deficient marine waters, in methods in enzymology. Elsevier, pp. 305–329. https://doi.org/10.1016/B978-0-12-407863-5.00016-2.

He, Y., Sen, B., Wang, G., 2023. Diversity and dynamics of microbial communities in marine ecosystems. Water 16, 31. https://doi.org/10.3390/w16010031.

Hernández-Magaña, E., Kraft, B., 2024. Nitrous oxide production and consumption by marine ammonia-oxidizing archaea under oxygen depletion. Front. Microbiol. 15, 1410251. https://doi.org/10.3389/fmicb.2024.1410251.

Hollibaugh, J.T., Gifford, S.M., Moran, M.A., Ross, M.J., Sharma, S., Tolar, B.B., 2014. Seasonal variation in the metratranscriptomes of a Thaumarchaeota population from SE USA coastal waters. ISME J. 8 (3), 685–698.

Huanca-Valenzuela, P., Fuchsman, C.A., Tully, B.J., Sylvan, J.B., Cram, J.A., 2025. Quantitative microbial taxonomy across particle size, depth, and oxygen concentration. Front. Microbiol. 16, 1552305.

Huang, X., Liu, L., Wen, T., Zhu, R., Zhang, J., Cai, Z., 2015. Illumina MiSeq investigations on the changes of microbial community in the fusarium oxysporum f. sp. cubense infected soil during and after reductive soil disinfestation. Microbiol. Res. 181, 33–42. https://doi.org/10.1016/j.micres.2015.08.004.

Huang, Y., Qu, W., Fan, Y., Wang, J., 2022. Archaeal diversity in the seawater of Changjiang River estuary reveals its adaptability to bottom seawaters. J. Oceanol. Limnol. 40, 1051–1069. https://doi.org/10.1007/s00343-021-1035-8.

Jiang, S.-Q., Yu, Y.-N., Gao, R.-W., Wang, H., Zhang, J., Li, R., Long, X.-H., Shen, Q.-R., Chen, W., Cai, F., 2019. High-throughput absolute quantification sequencing reveals the effect of different fertilizer applications on bacterial community in a tomato cultivated coastal saline soil. Sci. Total Environ. 687, 601–609. https://doi.org/10.1016/j.scitotenv.2019.06.105.

Jiao, N., Yang, Y., Koshikawa, H., Watanabe, M., 2002. Influence of hydrographic conditions on picoplankton distribution in the East China Sea. Aquat. Microb. Ecol. 30, 37–48. https://doi.org/10.3354/ame030037.

Karthäuser, C., Ahmerkamp, S., Marchant, H.K., Bristow, L.A., Hauss, H., Iversen, M.H., Kiko, R., Maerz, J., Lavik, G., Kuypers, M.M.M., 2021. Small sinking particles control anammox rates in the Peruvian oxygen minimum zone. Nat. Commun. 12, 3235. https://doi.org/10.1038/s41467-021-23340-4.

Kraft, B., Jehmlich, N., Larsen, M., Bristow, L.A., Könneke, M., Thamdrup, B., Canfield, D.E., 2022. Oxygen and nitrogen production by an ammonia-oxidizing archaeon. Science 375 (6576), 97–100.

Li, D., Wang, L., Jiang, F., Zeng, X., Xu, Q., Zhang, X., Zheng, Q., Shao, Z., 2024. Prokaryotic community structure and key taxa in the Arabian Sea's oxygen minimum zone. Front. Mar. Sci. 11, 1380819.

Lin, Z., Hu, J., Ye, L., Cui, Y., Wu, J., 2025. Long-term trends in summer hypoxia and associated driving factors in the Pearl River estuary. China. Mar. Pollut. Bull. 211, 117456. https://doi.org/10.1016/j.marpolbul.2024.117456.

Liu, J., Huang, F., Liu, J., Liu, X., Lin, R., Zhong, X., Austin, B., Zhang, X.H., 2023. Phylotype resolved spatial variation and association patterns of planktonic Thaumarchaeota in eastern Chinese marginal seas. Mar. Life Sci. Technol. 5 (2), 257–270.

Liu, Q., Tolar, B.B., Ross, M.J., Cheek, J.B., Sweeney, C.M., Wallsgrove, N.J., Popp, B., Hollibaugh, J.T., 2018. Light and temperature control the seasonal distribution of Thaumarchaeota in the South Atlantic bight. ISME J. 12 (6), 1473–1485.

Liu, S., Hou, C., Dong, C., Zhao, D., Chen, Q., Yang, J.-Y.T., Tang, K., 2024. Integrated multi-omics analyses reveal microbial community resilience to fluctuating low oxygen in the East China Sea. Environ. Res. 261. https://doi.org/10.1016/j.envres.2024.119764.

Long, A.M., Jurgensen, S.K., Petchel, A.R., Savoie, E.R., Brum, J.R., 2021. Microbial ecology of oxygen minimum zones amidst ocean deoxygenation. Front. Microbiol. 12, 748961. https://doi.org/10.3389/fmicb.2021.748961.

Martens-Habbena, W., Qin, W., 2022. Archaeal nitrification without oxygen. Science 375, 27–28. https://doi.org/10.1126/science.abn0373.

Murali, R., Pace, L.A., Sanford, R.A., Ward, L.M., Lynes, M.M., Hatzenpichler, R., Lingappa, U.F., Fischer, W.W., Gennis, R.B., Hemp, J., 2024. Diversity and evolution of nitric oxide reduction in bacteria and archaea. Proc. Natl. Acad. Sci. 121, e2316422121. https://doi.org/10.1073/pnas.2316422121.

Offre, P., Spang, A., Schleper, C., 2013. Archaea in biogeochemical cycles. Ann. Rev. Microbiol. 67, 437–457. https://doi.org/10.1146/annurev-micro-092412-155614.

Oschlies, A., 2021. A committed fourfold increase in ocean oxygen loss. Nat. Commun. 12 (1), 2307.
Pajares, S., Pelayo, M. del C., 2025. Phylogenetic diversity and distribution patterns of ammonia-oxidizing microorganisms in marine environments. Hydrobiologia. https://doi.org/10.1007/s10750-025-05878-2.
Pascal, L., Cloutier-Artiwat, F., Zanon, A., Wallace, D.W., Chaillou, G., 2025. New deoxygenation threshold for N_2 and N_2O production in coastal waters and sediments. Global Biogeochem. Cycles 39 (8) e2024GB008218.
Proctor, C., Coupel, P., Casciotti, K., Tremblay, J.E., Zakem, E., Arrigo, K.R., Mills, M.M., 2023. Light, ammonium, pH, and phytoplankton competition as environmental factors controlling nitrification. Limnol. Oceanogr. 68 (7), 1490–1503.
Qin, W., Heal, K.R., Ramdasi, R., Kobelt, J.N., Martens-Habbena, W., Bertagnolli, A.D., Amin, S.A., Walker, C.B., Urakawa, H., Könneke, M., Devol, A.H., Moffett, J.W., Armbrust, E.V., Jensen, G.J., Ingalls, A.E., Stahl, D.A., 2017. *Nitrosopumilus maritimus* gen. nov., sp. nov., *Nitrosopumilus cobalaminigenes* sp. nov., *Nitrosopumilus oxyclinae* sp. nov., and *Nitrosopumilus ureiphilus* sp. nov., four marine ammonia-oxidizing archaea of the phylum Thaumarchaeota. Int. J. Syst. Evol. Microbiol. 67 (12), 5067–5079.
Qin, W., Zheng, Y., Zhao, F., Wang, Y., Urakawa, H., Martens-Habbena, W., Liu, H., Huang, X., Zhang, X., Nakagawa, T., Mende, D.R., Bollmann, A., Wang, B., Zhang, Y., Amin, S.A., Nielsen, J.L., Mori, K., Takahashi, R., Virginia Armbrust, E., Winkler, M.-K.H., DeLong, E.F., Li, M., Lee, P.-H., Zhou, J., Zhang, C., Zhang, T., Stahl, D.A., Ingalls, A.E., 2020. Alternative strategies of nutrient acquisition and energy conservation map to the biogeography of marine ammonia-oxidizing archaea. ISME J. 14, 2595–2609. https://doi.org/10.1038/s41396-020-0710-7.
Qin, W., Wei, S.P., Zheng, Y., Choi, E., Li, X., Johnston, J., Wan, X., Abrahamson, B., Flinkstrom, Z., Wang, B., Li, H., Hou, L., Tao, Q., Chlouber, W., Sun, X., Wells, M., Ngo, L., Hunt, K., Urakawa, H., Tao, X., Wang, D., Yan, X., Wang, D., Pan, C., Weber, P., Jiang, J., Zhou, J., Zhang, Y., Stahl, D., Ward, B., Mayali, X., Willm Martens-Habbena, W., Winkler, M., 2024. Ammonia-oxidizing bacteria and archaea exhibit differential nitrogen source preferences. Nat. Microbiol. 9 (2), 524–536.
Ren, M., Wang, J., 2022. Phylogenetic divergence and adaptation of Nitrososphaeria across lake depths and freshwater ecosystems. ISME J. 16 (6), 1491–1501.
Reyes, C., Hodgskiss, L.H., Kerou, M., Pribasnig, T., Abby, S.S., Bayer, B., Kraemer, S.M., Schleper, C., 2020. Genome wide transcriptomic analysis of the soil ammonia oxidizing archaeon Nitrososphaera viennensis upon exposure to copper limitation. ISME J. 14, 2659–2674. https://doi.org/10.1038/s41396-020-0715-2.
Rose, K.C., Ferrer, E.M., Carpenter, S.R., Crowe, S.A., Donelan, S.C., Garçon, V.C., Grégoire, M., Jane, S.F., Leavitt, P.R., Levin, L., Oschlies, A., Breitburg, D., 2024. Aquatic deoxygenation as a planetary boundary and key regulator of earth system stability. Nat. Ecol. Evol. 8 (8), 1400–1406.
Santoferrara, L., McManus, G., Greenfield, D., Smith, S., 2022. Microbial communities (bacteria, archaea and eukaryotes) in a temperate estuary during seasonal hypoxia. Aquat. Microb. Ecol. 88, 61–79. https://doi.org/10.3354/ame01982.
Schiebenhoefer, H., Schallert, K., Renard, B.Y., Trappe, K., Schmid, E., Benndorf, D., Riedel, K., Muth, T., Fuchs, S., 2020. A complete and flexible workflow for metaproteomics data analysis based on MetaProteomeAnalyzer and Prophane. Nat. Protoc. 15, 3212–3239. https://doi.org/10.1038/s41596-020-0368-7.
Semedo, M., Lopes, E., Baptista, M.S., Oller-Ruiz, A., Gilabert, J., Tomasino, M.P., Magalhães, C., 2021. Depth profile of nitrifying archaeal and bacterial communities in the remote oligotrophic waters of the North Pacific. Front. Microbiol. 12, 624071.
Sheng, H., Darby, S.E., Zhao, N., Liu, D., Kettner, A.J., Lu, X., Yang, Y., Gao, J.H., Zhao, Y.Q., Wang, Y.P., 2024. Anthropogenic eutrophication and stratification strength control hypoxia in the Yangtze estuary. Commun. Earth Environ. 5 (1), 235.
Song, H., Wignall, P.B., Song, H., Dai, X., Chu, D., 2019. Seawater temperature and dissolved oxygen over the past 500 million years. J. Earth Sci. 30, 236–243. https://doi.org/10.1007/s12583-018-1002-2.
Stahl, D.A., De La Torre, J.R., 2012. Physiology and diversity of ammonia-oxidizing archaea. Ann. Rev. Microbiol. 66, 83–101. https://doi.org/10.1146/annurev-micro-092611-150128.
Stein, L.Y., 2019. Insights into the physiology of ammonia-oxidizing microorganisms. Curr. Opin. Chem. Biol. 49, 9–15. https://doi.org/10.1016/j.cbpa.2018.09.003.
Straka, L.L., Meinhardt, K.A., Bollmann, A., Stahl, D.A., Winkler, M.-K.H., 2019. Affinity informs environmental cooperation between ammonia-oxidizing archaea (AOA) and anaerobic ammonia-oxidizing (Anammox) bacteria. ISME J. 13, 1997–2004. https://doi.org/10.1038/s41396-019-0408-x.
Sun, Y., 2024. Dynamics of nutrient cycles in the Permian-Triassic oceans. Earth Sci. Rev. 258, 104914. https://doi.org/10.1016/j.earscirev.2024.104914.
Sveen, T.R., Hannula, S.E., Bahram, M., 2024. Microbial regulation of feedbacks to ecosystem change. Trends Microbiol. 32 (1), 68–78.
Tang, W., Fortin, S.G., Intrator, N., Lee, J.A., Kunes, M.A., Jayakumar, A., Haynes, S., Oleynik, S., Sigman, D., Ward, B., 2025. Similar oxygen sensitivities of different steps of denitrification in estuarine waters. Environ. Sci. Technol. 59 (14), 7165–7175.
Teeling, H., Fuchs, B.M., Becher, D., Klockow, C., Gardebrecht, A., Bennke, C.M., Kassabgy, M., Huang, S., Mann, A.J., Waldmann, J., Weber, M., Klindworth, A., Otto, A., Lange, J., Bernhardt, J., Reinsch, C., Hecker, M., Peplies, J., Bockelmann, F. D., Callies, U., Gerdts, G., Wichels, A., Wiltshire, K.H., Glöckner, F.O., Schweder, T., Amann, R., 2012. Substrate-controlled succession of marine bacterioplankton populations induced by a phytoplankton bloom. Science 336, 608–611. https://doi.org/10.1126/science.1218344.
Thrash, A., Arick, M., Peterson, D.G., 2018. Quack: a quality assurance tool for high throughput sequence data. Anal. Biochem. 548, 38–43. https://doi.org/10.1016/j.ab.2018.01.028.
Tkacz, A., Hortala, M., Poole, P.S., 2018. Absolute quantitation of microbiota abundance in environmental samples. Microbiome 6, 110. https://doi.org/10.1186/s40168-018-0491-7.
Walters, W., Hyde, E.R., Berg-Lyons, D., Ackermann, G., Humphrey, G., Parada, A., Gilbert, J.A., Jansson, J.K., Caporaso, J.G., Fuhrman, J.A., Apprill, A., Knight, R., 2016. Improved bacterial 16S rRNA gene (V4 and V4-5) and fungal internal transcribed spacer marker gene primers for microbial community surveys. mSystems 1, e00009–e00015. https://doi.org/10.1128/mSystems.00009-15.
Wan, X.S., Sheng, H.X., Dai, M., Church, M.J., Zou, W., Li, X., Hutchins, D., Ward, B.B., Kao, S.J., 2021. Phytoplankton-nitrifier interactions control the geographic distribution of nitrite in the upper ocean. Global Biogeochem. Cycles 35 (11) e2021GB007072.
Wan, X.S., Hou, L., Kao, S.J., Zhang, Y., Sheng, H.X., Shen, H., Tong, S., Qin, W., Ward, B. B., 2023. Pathways of N_2O production by marine ammonia-oxidizing archaea determined from dual-isotope labeling. Proc. Natl. Acad. Sci. 120 (11), e2220697120.
Wang, K., Yao, J., Wang, J., Liu, H., Yin, K., 2022. Role of winds in interrupting the formation of coastal hypoxia. Front. Mar. Sci. 9, 839812. https://doi.org/10.3389/fmars.2022.839812.
Wang, Z., Xue, C., Ping, B., 2024. A reconstructing model based on time-space-depth partitioning for global ocean dissolved oxygen concentration. Remote Sens. 16, 228. https://doi.org/10.3390/rs16020228.
Wolf, S., Jayawickrama, C., Carlson, C.A., Deutsch, C., Davis, E.W., Daniels, B.N., Chan, F., Giovannoni, S.J., 2025. Microbial carbon oxidation in seawater below the hypoxic threshold. Sci. Rep. 15, 2838. https://doi.org/10.1038/s41598-024-82438-z.
Xie, W., Luo, H., Murugapiran, S.K., Dodsworth, J.A., Chen, S., Sun, Y., Hedlund, B.P., Wang, P., Fang, H., Deng, M., Zhang, C.L., 2018. Localized high abundance of marine group II archaea in the subtropical Pearl River estuary: implications for their niche adaptation. Environ. Microbiol. 20, 734–754. https://doi.org/10.1111/1462-2920.14004.
Zhang, J., Zhu, X., Zhang, R., Ren, J., Wu, Y., Liu, S., Huang, D., 2022. Dissolved Fe in the East China Sea under the influences of land sources and the boundary current with implications for global marginal seas. Global Biogeochem. Cycles 36 e2021GB006946.
Zhang, R.Y., Wang, Y.R., Liu, R.L., Rhee, S.K., Zhao, G.P., Quan, Z.X., 2024a. Metagenomic characterization of a novel non-ammonia-oxidizing Thaumarchaeota from hadal sediment. Microbiome 12 (1), 7.
Zhang, W., Moriarty, J.M., Wu, H., Feng, Y., 2021. Response of bottom hypoxia off the Changjiang River estuary to multiple factors: a numerical study. Ocean Model 159, 101751. https://doi.org/10.1016/j.ocemod.2021.101751.
Zhang, W., Zhou, F., Huang, D., Chen, J., Zhu, J., 2023. Mechanisms controlling interannual variability of seasonal hypoxia off the Changjiang River estuary. J. Geophys. Res. Oceans 128 (10) e2023JC019996.
Zhang, Z., Zhang, Q., Chen, B., Yu, Y., Wang, T., Xu, N., Fan, X., Penuelas, J., Fu, Z.W., Deng, Y., Zhu, Y.G., Qian, H., 2024b. Global biogeography of microbes driving ocean ecological status under climate change. Nat. Commun. 15 (1), 4657.
Zheng, Q., Wang, Y., Lu, J., Lin, W., Chen, F., Jiao, N., 2020. Metagenomic and Metaproteomic insights into photoautotrophic and heterotrophic interactions in a *Synechococcus* culture. Mbio 11. https://doi.org/10.1128/mBio.03261-19 e03261–19.
Zhou, F., Chai, F., Huang, D., Wells, M., Ma, X., Meng, Q., Xue, H., Xuan, J., Wang, P., Ni, X., Zhao, Q., Liu, C., Su, J., Li, H., 2020. Coupling and decoupling of high biomass phytoplankton production and hypoxia in a highly dynamic coastal system: the Changjiang (Yangtze River) estuary. Front. Mar. Sci. 7, 259. https://doi.org/10.3389/fmars.2020.00259.
Zou, D., Liu, H., Li, M., 2020. Community, distribution, and ecological roles of estuarine archaea. Front. Microbiol. 11, 2060. https://doi.org/10.3389/fmicb.2020.02060.
Zou, D., Li, H., Du, P., Wang, B., Lin, H., Liu, H., Chen, J., Li, M., 2022. Distinct features of sedimentary archaeal communities in hypoxia and non-hypoxia regions off the Changjiang River estuary. Microbiol. Spect. 10 (5) e01947–22.